Supporting Information for

Spotting d-band centers of single-atom catalysts by oxygen intermediate-boosted electrochemiluminescence

Ruyu Xie,[a] Kaitao Li,[ac] Rui Tian,*[ac] and Chao Lu*[abc]

[a]*State Key Laboratory of Chemical Resource Engineering, Beijing University of Chemical Technology, Beijing, 100029, China*

[b]*Pingyuan Laboratory, College of Chemistry, Zhengzhou University, Zhengzhou, 450001, China*

[c]*Quzhou Institute for Innovation in Resource Chemical Engineering, Quzhou, 324000, China*

*E-mail: tianrui@mail.buct.edu.cn; luchao@mail.buct.edu.cn

Table of Contents

Experimental Section

Materials. $Co(NO_3)_2 \cdot 6H_2O$ (analytical reagent), NH_4F (analytical reagent) and urea (chemical pure) were all acquired from Xilong Scientific Co. Ltd. (Guangdong, China). $Al(NO_3)_3 \cdot 9H_2O$ (analytical reagent), HCl, dimethyl sulfoxide (DMSO), KOH (AR), and Na_2HPO_4 (AR) were obtained from Beijing Reagent Company (Beijing, China). NaH_2PO_4 (guaranteed reagent) was purchased from Tianjin Jinke Fine Chemical Research Institute (Tianjin, China). NaN_3 (analytical reagent) was obtained from Fuchen Chemical Reagent Co., Ltd. (Tianjin, China). *p*-Benzoquinone (BQ, chemical pure) was supplied by Sinopharm Chemical Reagent Co., Ltd. (Shanghai, China). 2-Propanol (>99.7%) and isopropyl alcohol (IPA) (>99.7%) were acquired from Shanghai Tian Scientific Co., Ltd. (Shanghai, China). Indium tin oxide (ITO) electrodes (transmittance > 84%) were supplied by South China Science & Technology Company Limited (Shenzhen, China). Chloroauric acid tetrahydrate ($HAuCl_4 \cdot xH_2O$) was purchased from Damas-beta (Shanghai, China). $AgNO_3$ (analytical reagent >99.8%) was bought from Beijing HWRK Company (Beijing, China). Nitro blue tetrazolium chloride (NBT) was obtained by Tokyo Chemical Industry Co., Ltd. (Tokyo, Japan). Luminol (> 98.0%) was supplied from Tokyo Chemical Industry Co., Ltd. (Tokyo, Japan). All the above reagents were used without further treatment.

Preparation of CoAl/LDHs on indium tin oxide (ITO) electrodes. ITO electrodes with the size of 1 × 2 cm^2 were firstly activated in ethanol and water under ultrasonic treatment for 15 minutes. The CoAl/LDHs was synthesized on ITO electrodes through a one-pot hydrothermal method according to the previous report with slight modification.[1] Brifly, $Co(NO_3)_2 \cdot 6H_2O$ (0.165 mmol), $Al(NO_3)_3 \cdot 9H_2O$ (0.55 mmol), NH_4F (0.8 mmol) and urea (2.0 mmol) were dissolved in 16.0 mL of deionized water and then transferred to a 25 mL Teflon-lined stainless steel autoclave. Next, the treated electrodes were placed vertically in the autoclave, and the CoAl/LDHs were prepared on the ITO electrodes. The hydrothermal reaction was carried out at 120 °C for 6 hours. After cooling to the room temperature, the electrodes with deposited CoAl/LDHs (labelled as LDH/ITO) were washed with deionized water and dried in air, and the acuiqred LDH/ITO was employed as the working electrode.

Preparation of LDH/ITO-supported single atoms. Electrodeposition method was employed to immobilize single atoms onto CoAl/LDH support.[2] Taking Ag^s/LDH/ITO as an example, a typical three-electrode system was employed. Briefly, LDH/ITO, Ag/AgCl and Pt electrodes were used as working electrode, reference electrode and counter electrode, respectively. The working electrolyte was 100.0 mL of KOH aqueous solution (1.2 mol/L), containing 0.1 mmol/L $AgNO_3$ as the precursor for Ag species. The electrochemical depositions were carried out by cycling the potentials from −0.556 to −0.156 V with a scanning rate of 50 mV s^{-1} under

stirring for 2 cycles, and the stirring rate was set as 600 r/min. After washing with deionized water, the Ag single atoms were localized onto the LDH/ITO electrodes and marked as Ag^s/LDH/ITO.

Similarly, Au^s/LDH/ITO, Cu^s/LDH/ITO and Fe^s/LDH/ITO were prepared through the electrodeposition method taking $HAuCl_4 \cdot xH_2O$, $FeCl_3$ and $CuCl_2$ as the metal precursors, respectively. The working electrolyte contained 100 μmol/L metal precursor and 1.2 mol/L KOH.

Preparation of controlled samples on ITO electrodes. To prepare Au or Ag nanoparticles, electrodeposition of 30 cycles were employed. In detail, Ag^{np}/ITO and Au^{np}/ITO electrodes were acquired through the electrodeposition on bare ITO electrodes in KOH aqueous solution (1.2 mol/L) containing 0.1 mmol/L $AgNO_3$ or 0.1 mmol/L $HAuCl_4 \cdot xH_2O$, respectively. Similarly, the Ag or Au nanoparticles were immobilized on the LDH/ITO electrodes under the same condition of electrodeposition to acquire Ag^{np}/LDH/ITO and Au^{np}/LDH/ITO samples.

Electrochemical and electrochemiluminescence measurements. A CHI660E electrochemical workstation was used to perform the electrochemical experiments in a traditional three-electrode system with Pt, Ag/AgCl and modified ITO as counter electrode, reference electrode and the working electrode. The effective surface area of the working electrode was measured as 1 × 1

cm^2 during the electrochemical deposition and ECL measurements. Cyclic voltammetry (CV) curves were recorded in 6.0 mL of 0.01 mmol luminol (phosphate-buffered saline, PBS, pH = 7.5) in a potential range from −0.8 to +0.8 V at a scan rate of 0.1 V/s. Real-time electrochemiluminescence (ECL) signals were collected by a biophysics chemiluminescence analyzer (Institute of Biophysics, Chinese Academy of Sciences, Beijing, China) with the voltage of the photomultiplier tube at −900 V. The I_{ECL}−potential curves were obtained based on the combination of the CV signal from CHI660E electrochemical workstation and ECL signal collected by a biophysics CL analyzer. The ECL emission spectra were acquired by an F-7000 fluorescence spectrophotometer (Hitachi, Tokyo, Japan) coupled with CHI660E. Electrochemical impedance spectroscopy (EIS) measurements were carried out from 0.1 Hz to 100 kHz in 5.0 mmol/L $K_3[Fe(CN)_6]/K_4[Fe(CN)_6]$ (0.1 mol/L KCl). The linear sweep voltammetry (LSV) curves were recorded at different rotation rates in O_2-saturated 0.1 mol/L PBS (pH = 7.5) from 0 V to −1.2 V with a sweeping rate of 5 mV/s.

The identification of radicals during the ECL reaction were studied by a radical trapping experiment. Briefly, 70 μL of NaN_3, IPA and BQ (0.02 mol/L) solution were added to 6.0 mL of 0.01 mmol/L luminol to capture singlet oxygen ($^1O_2$), superoxide radical ($O_2^{\bullet-}$), and hydroxyl radical (OH•), respectively. $O_2^{\bullet-}$ was semi-quantitatively analyzed by the trapping experiment of NBT. 100 μL of NBT (20 μmol/L) was added to the luminol electrolyte, and scans in the range of −0.8 to +0.8 V were performed for 10 times to produce $O_2^{\bullet-}$. The resulting electrode was

dissolved in 10 mL of 0.5% KOH-dimethyl sulfoxide solution for UV-vis adsorption measurement.

Sample characterization. X-ray diffraction (XRD) patterns for the samples were recorded with a 2500VB2 (Rigaku Corporation, Japan) using a Cu Kα (radiation λ = 1.541 844 Å) ranging from 3° to 90° under a scanning rate of 5°/min. X-ray photoelectron spectroscopy (XPS) and ultraviolet photoelectron spectroscopy (UPS) measurements were implemented using an ESCALAB-MKII 250 (Thermo, Waltham, U.S.A.) with an Al K as exciting source. Scanning electron microscopy (SEM) images were taken on a JSM-7800F (Japan Electron Optics Laboratory Co., Ltd.) scanning electron microscope. High-resolution transmission electron microscopy (HRTEM) images were obtained with a JEM-ARM200F (Japan Electron Optics Laboratory Co., Ltd.). The morphologies of Au and Ag nanoparticles were studied by TEM 2100 (Japan Electron Optics Laboratory Co., Ltd.). High-angle annular dark-field scanning transmission electron microscopy (HAADF-STEM) was performed on a JEOL JEM-ARM200F equipped with double aberration correctors and a cold field emission gun. The mass loadings of samples on the modified electrodes were analyzed by inductively coupled plasma optical emission spectrometry (ICP-OES, Thermo Fisher Scientific, U.S.A.). UV-vis absorption spectra were acquired by a UV-3900H (Shimadzu, Tokyo, Japan) spectrophotometer. Temperature-programmed desorption (TPD) was performed on a micromeritics chemisorb 2750

chemisorption instrument (ChemBET Pulsar, USA) with a thermal conductivity detector. The samples of 0.1000 g were preheated in a gas stream (10% oxygen and 90% helium) at 120 °C for 1 h. After cooling to the room temperature, the samples were kept in the same gas stream for 1 h to ensure saturated adsorption and then purged with a helium stream for another 1 h. The O_2-TPD curve was collected by ramping the temperature from 30 °C to 950 °C with helium flow as the carrier gas (40 mL/min).

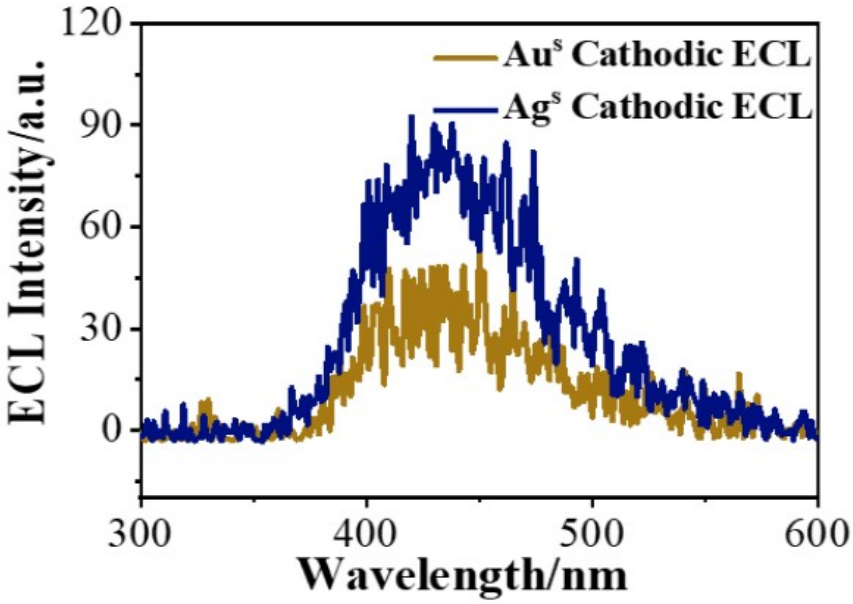

Fig. S1 Cathodic electrochemiluminescence (ECL) spectra at Ag^s/LDH/ITO or Au^s/LDH/ITO electrode in 0.01 mmol/L luminol (PBS, pH = 7.5).

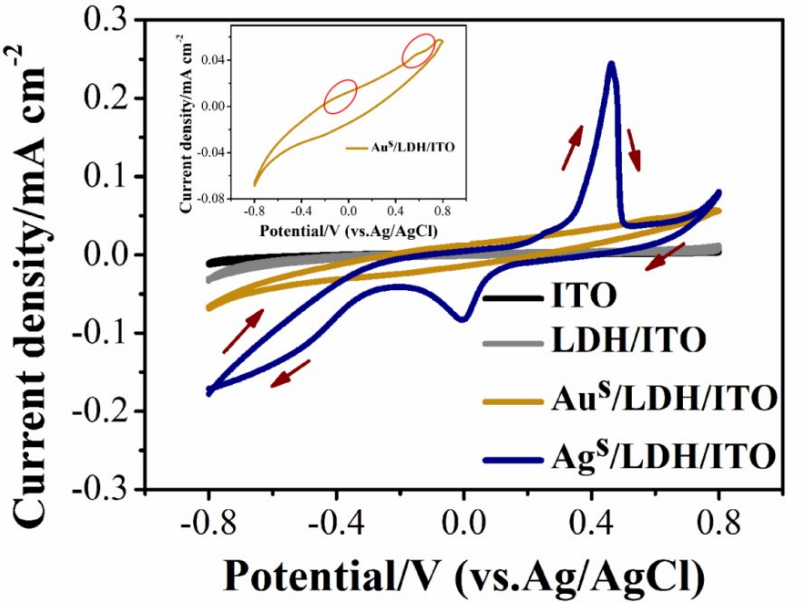

Fig. S2 Current density-voltammetry curves in 0.01 mmol/L luminol (PBS, pH = 7.5) at ITO, LDH/ITO, Au^s/LDH/ITO and Ag^s/LDH/ITO electrodes.

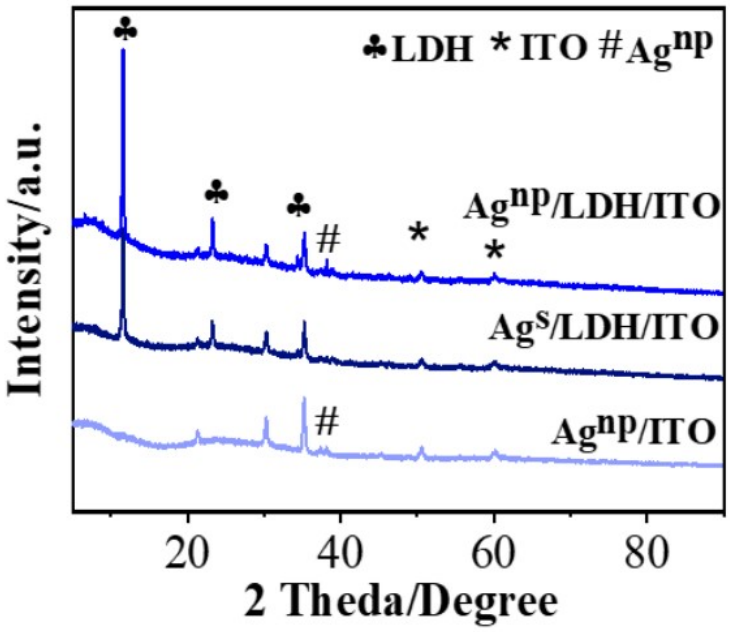

Fig. S3 X-ray diffraction (XRD) patterns of Ag^{np}/LDH/ITO, Ag^{s}/LDH/ITO and Ag^{np}/ITO samples.

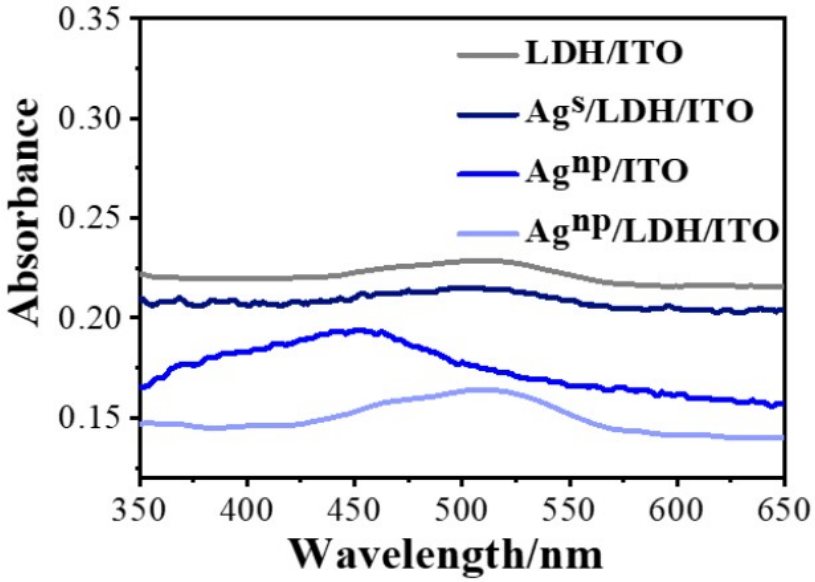

Fig. S4 UV-vis absorption spectra of LDH/ITO, Ag^{np}/ITO, Ag^{np}/LDH/ITO and Ag^{s}/LDH/ITO samples.

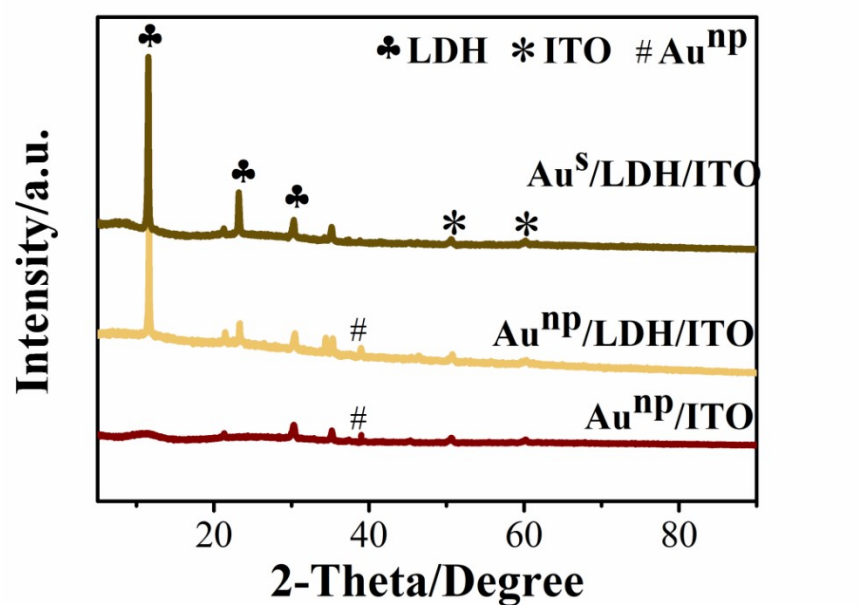

Fig. S5 XRD patterns of Au^{s}/LDH/ITO, Au^{np}/LDH/ITO and Au^{np}/ITO samples.

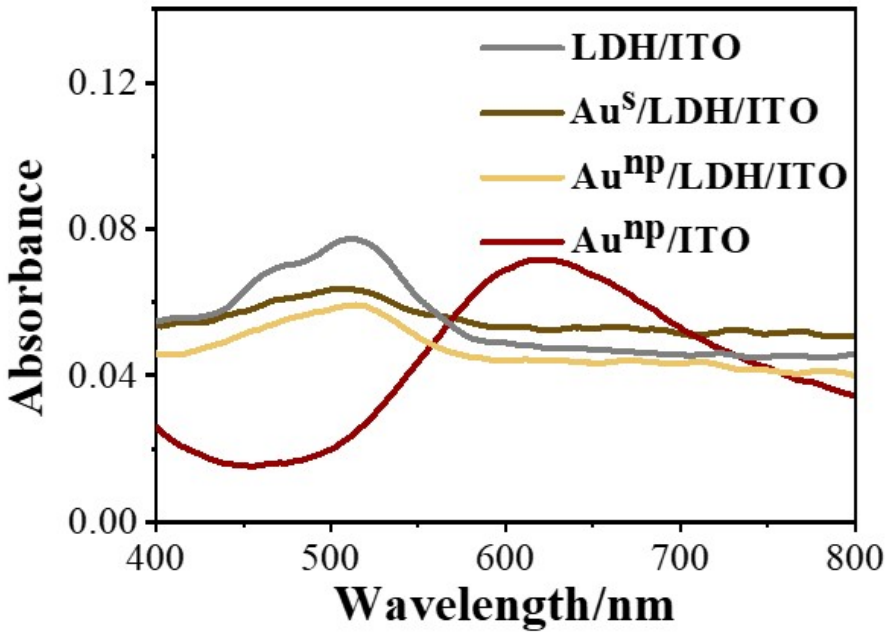

Fig. S6 UV-vis absorption spectra of Au^{s}/LDH/ITO, Au^{np}/ITO, Au^{np}/LDH/ITO and LDH/ITO samples.

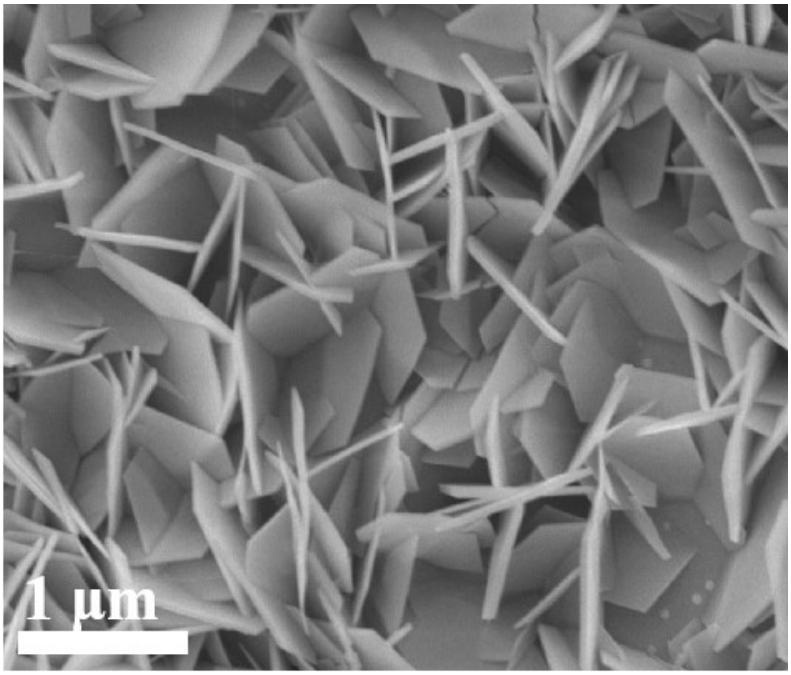

Fig.S7 Scanning electron microscopy (SEM) image of CoAl/LDH deposited on ITO electrode.

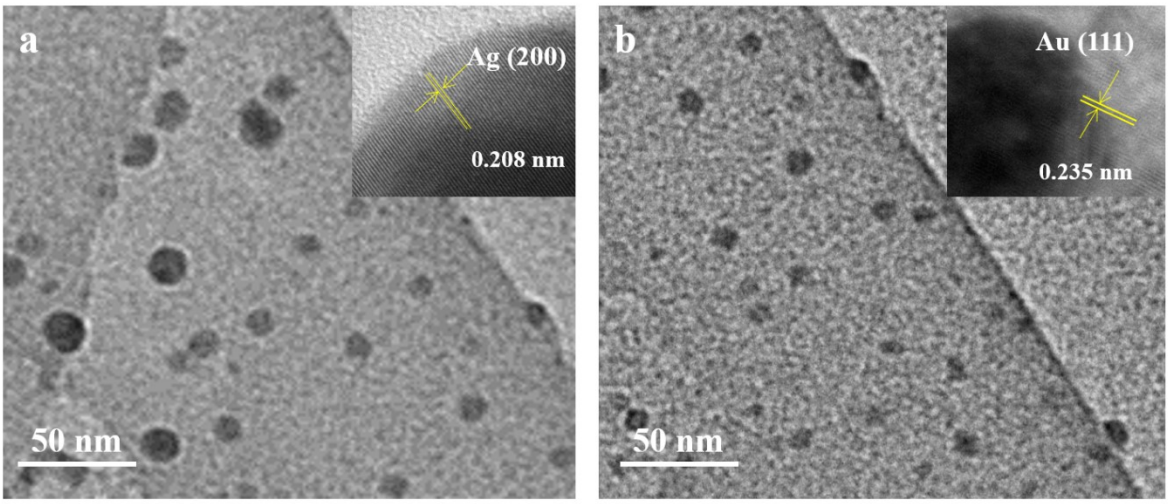

Fig. S8 Transmission electron microscopy (TEM) images and the high-resolution TEM images (insets) of (a) Ag^{np}/LDH/ITO and (b) Au^{np}/LDH/ITO.

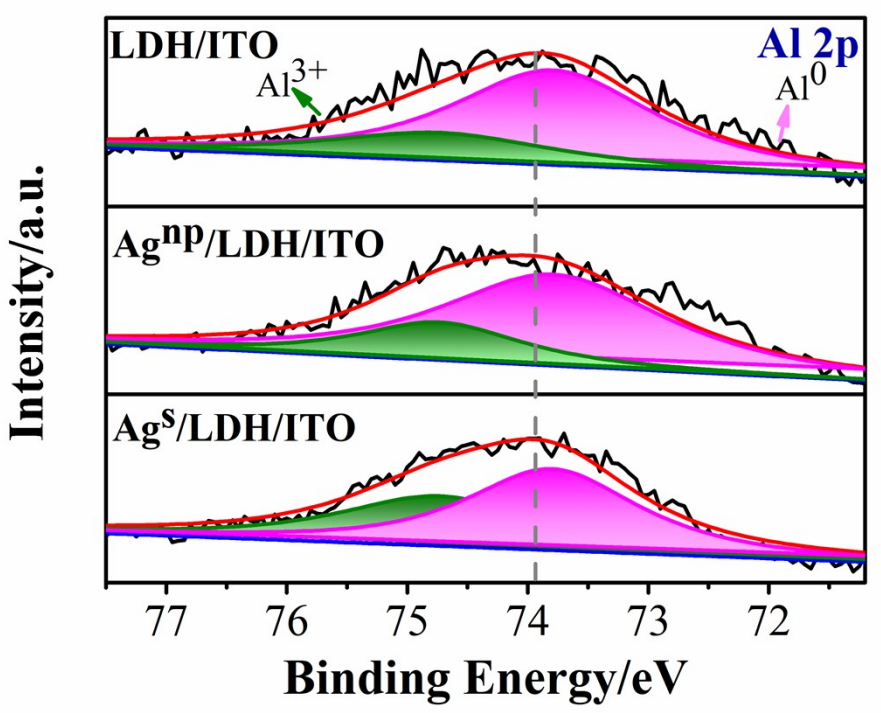

Fig. S9 X-ray photoelectron spectroscopy (XPS) spectra of Al 2p for LDH/ITO, Ag^{np}/LDH/ITO and Ag^{s}/LDH/ITO.

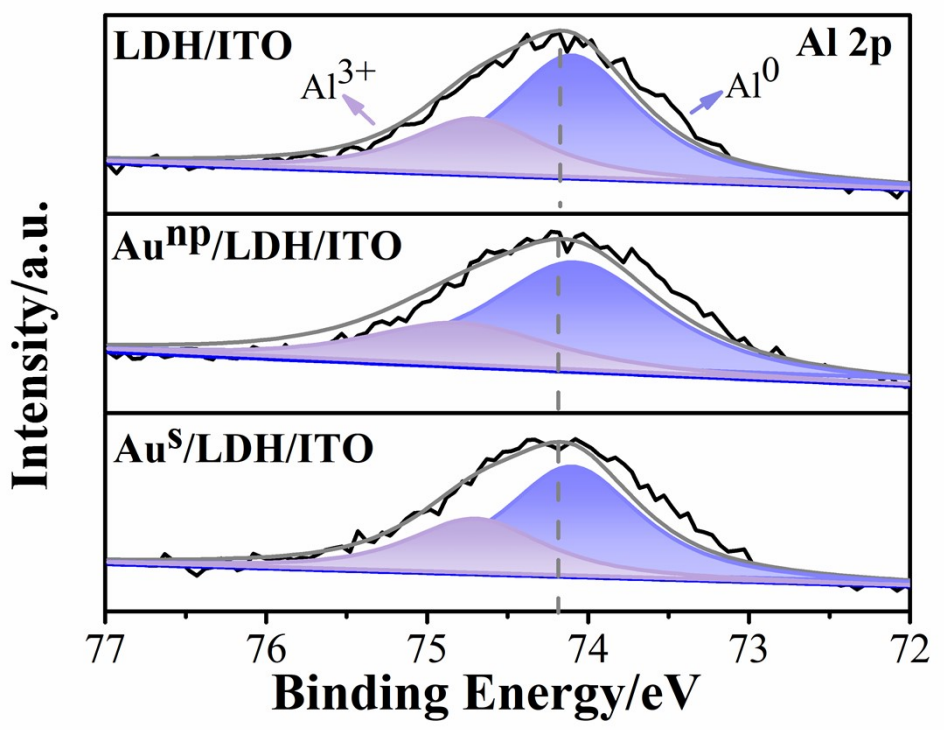

Fig. S10 XPS spectra of Al 2p for LDH/ITO, Au^{np}/LDH/ITO and Au^{s}/LDH/ITO.

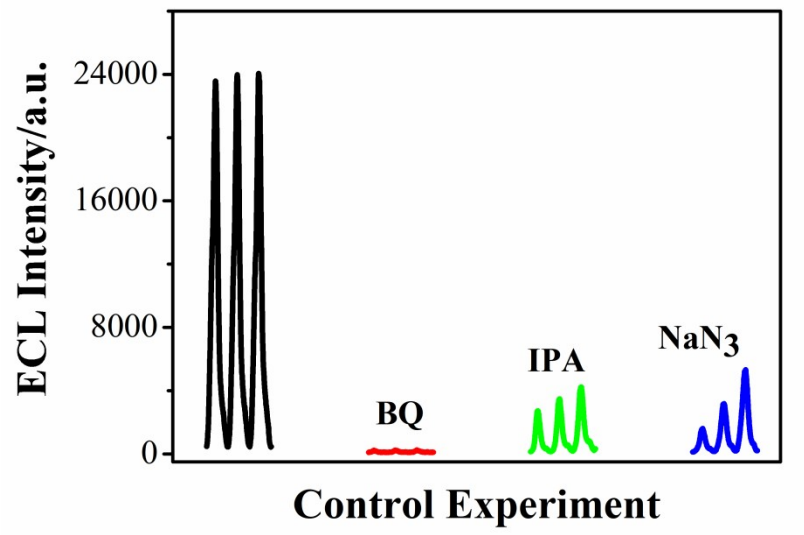

Fig. S11 ECL intensities at Ag^s/LDH/ITO electrode in the absence (black lines) or presence of *p*-Benzoquinone (BQ, red lines), isopropyl alcohol (IPA, green lines), and NaN_3 (blue lines) as radical scavengers, respectively (the potential ranged from –0.8 V to 0 V).

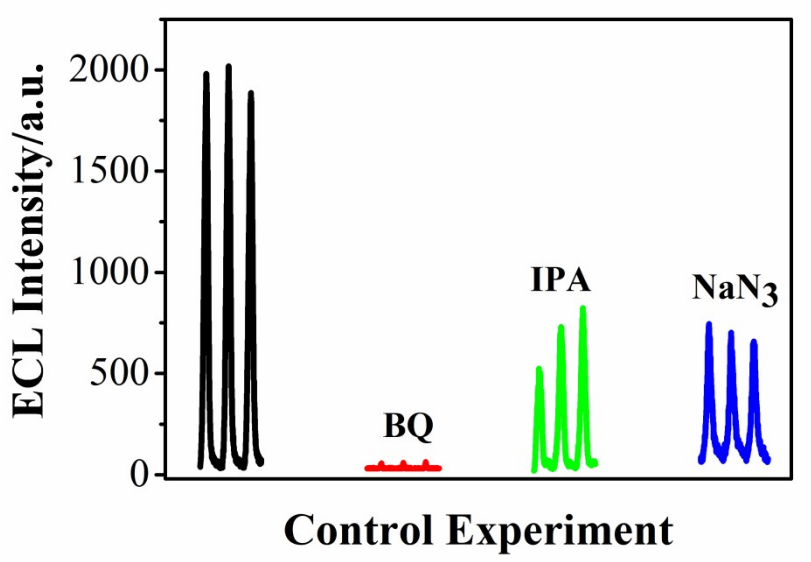

Fig. S12 ECL intensities at Au^s/LDH/ITO electrode in the absence (black lines) or presence of *p*-BQ (red lines), IPA (green lines), and NaN_3 (blue lines) as radical scavengers, respectively (the potential ranged from –0.8 V to 0 V).

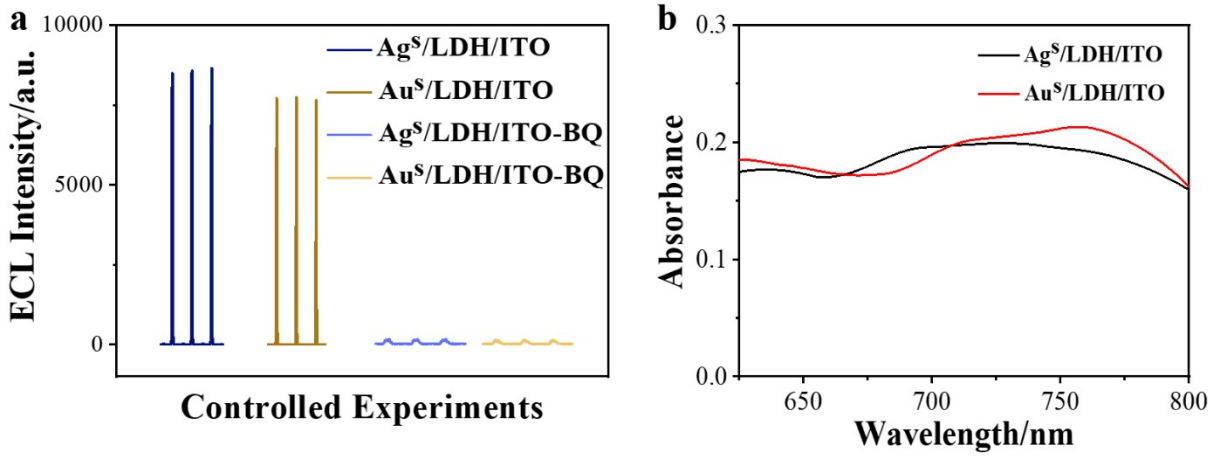

Fig. S13 (a) ECL intensities at Ag^s/LDH/ITO and Au^s/LDH/ITO electrodes in the absence or presence of *p*-BQ as radical scavengers, and (b) UV-vis spectra of NBT for the Ag^s/LDH/ITO and Au^s/LDH/ITO electrodes in KOH/DMSO solutions (the potential ranged from 0 V to +0.8 V).

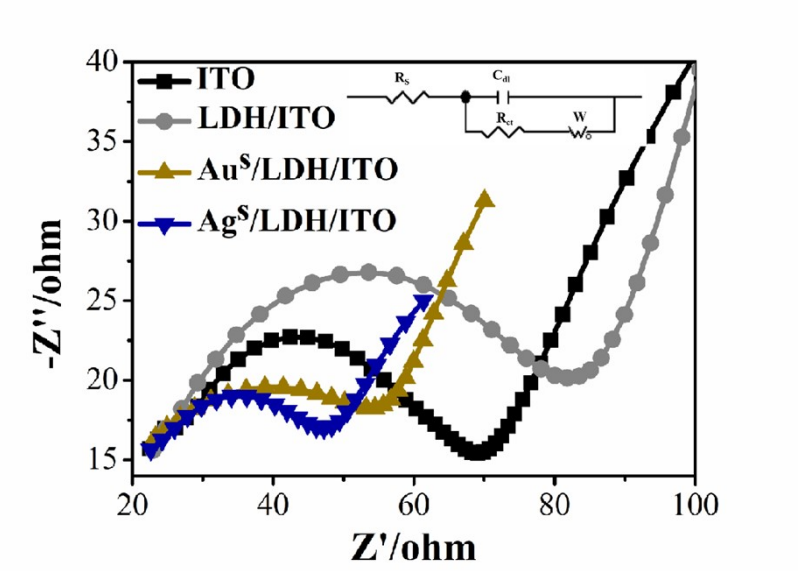

Fig. S14 Electrochemical impedance spectroscopy (EIS) results for ITO, LDH/ITO, Au^s/LDH/ITO and Ag^s/LDH/ITO electrodes, and the inset showed the equivalent circuit (R_s, R_{ct}, C_{dl}, and W represented the resistance of solution, charge transfer resistance, double layer capacitance, and the Warburg constant, respectively).

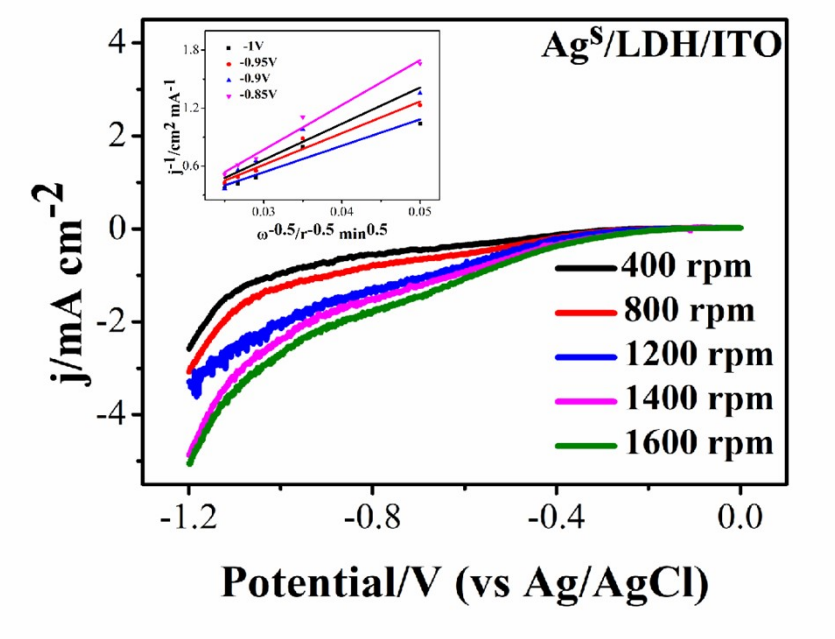

Fig. S15 Linear sweep voltammetry (LSV) curves of Ag^s/LDH/ITO electrode in O_2-saturated PBS (pH = 7.5) solution at different rotation rates (the inset showed the K-L plots of j^{-1} vs. $\omega^{-1/2}$ at different potentials).

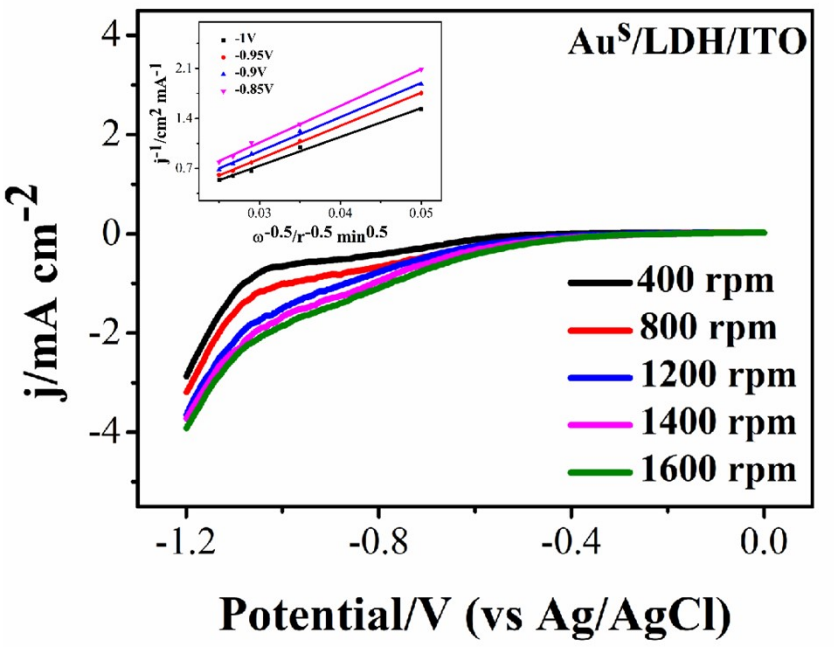

Fig. S16 LSV curves of Au^s/LDH/ITO electrode in O_2-saturated PBS (pH = 7.5) solution at different rotation rates (the inset showed the K-L plots of j^{-1} vs. $\omega^{-1/2}$ at different potentials).

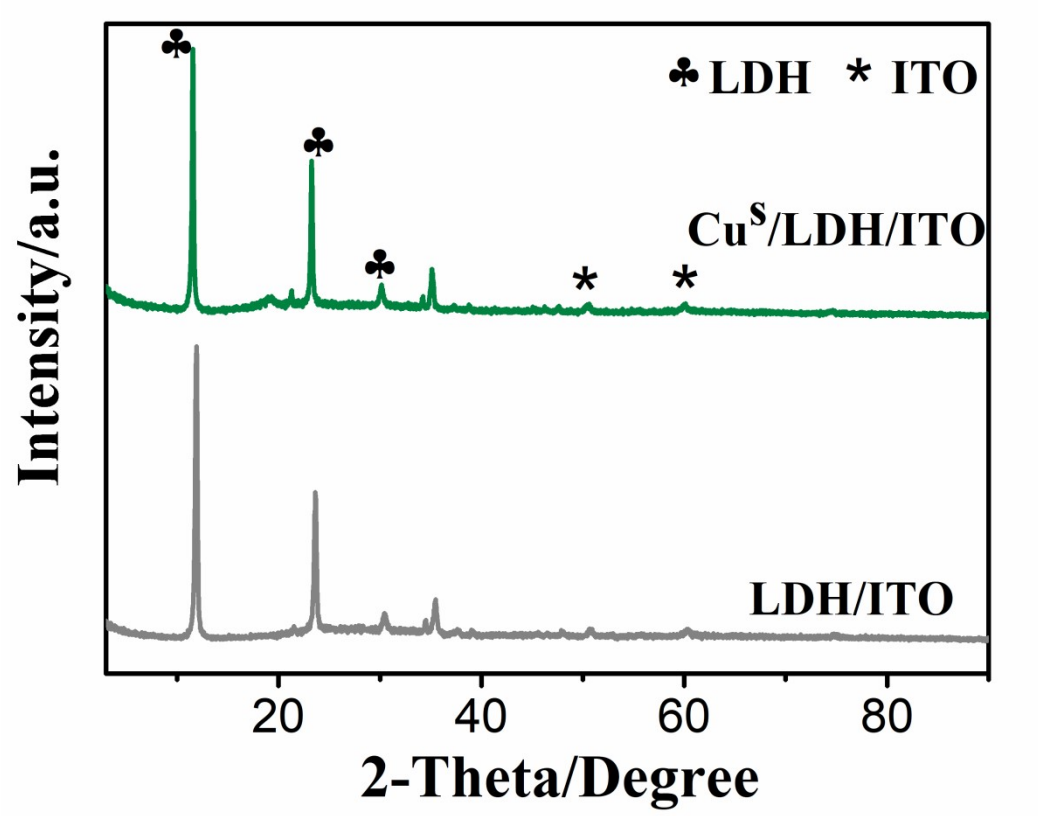

Fig. S17 XRD patterns of Cu^s/LDH/ITO and LDH/ITO samples (absence of Cu nanoparticles at 50°).

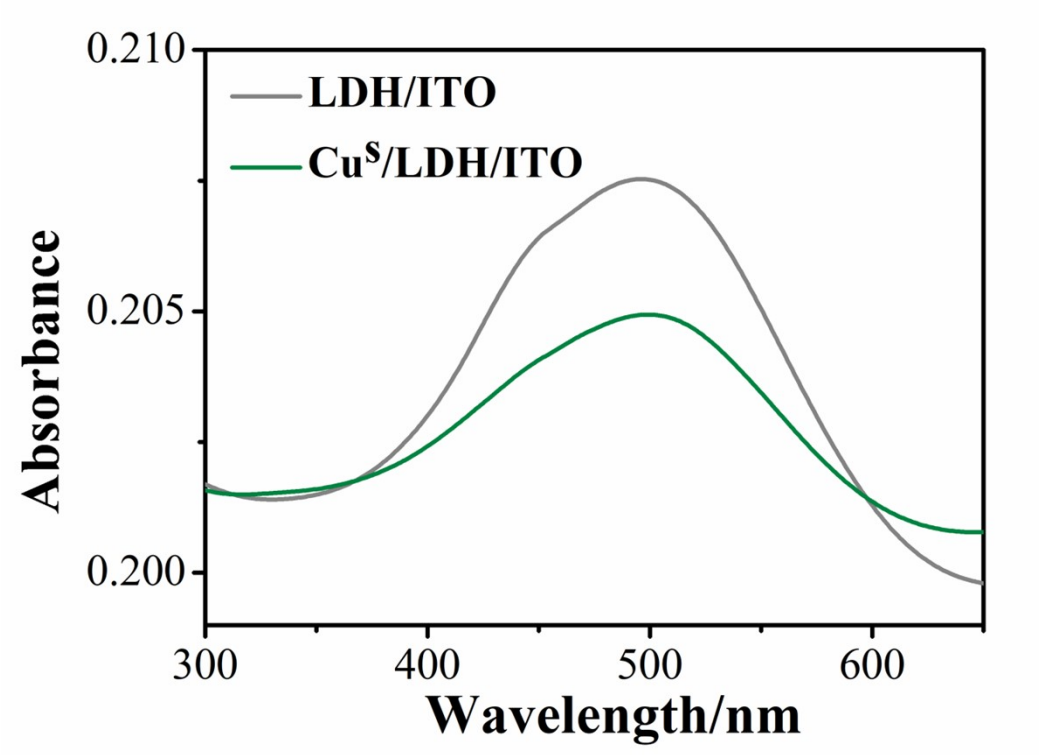

Fig. S18 UV-vis absorption spectra of Cu^s/LDH/ITO and LDH/ITO samples (absence of Cu nanoparticles at 330 nm).

.

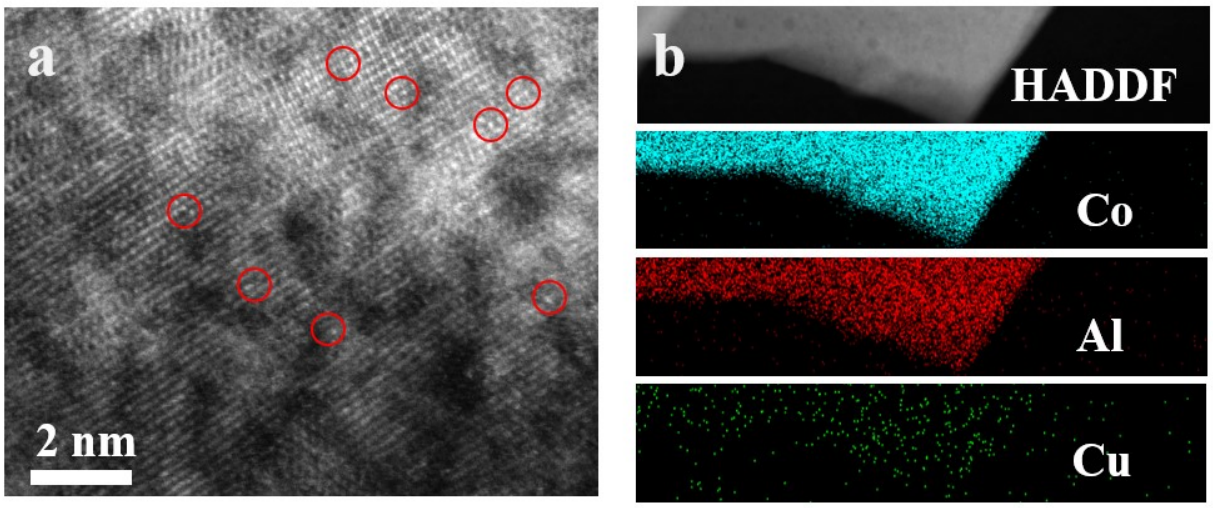

Fig. S19 (a) HAADF-STEM image and (b) STEM-EDS mapping images of Co, Al, and Cu for Cu^{s}/LDH/ITO.

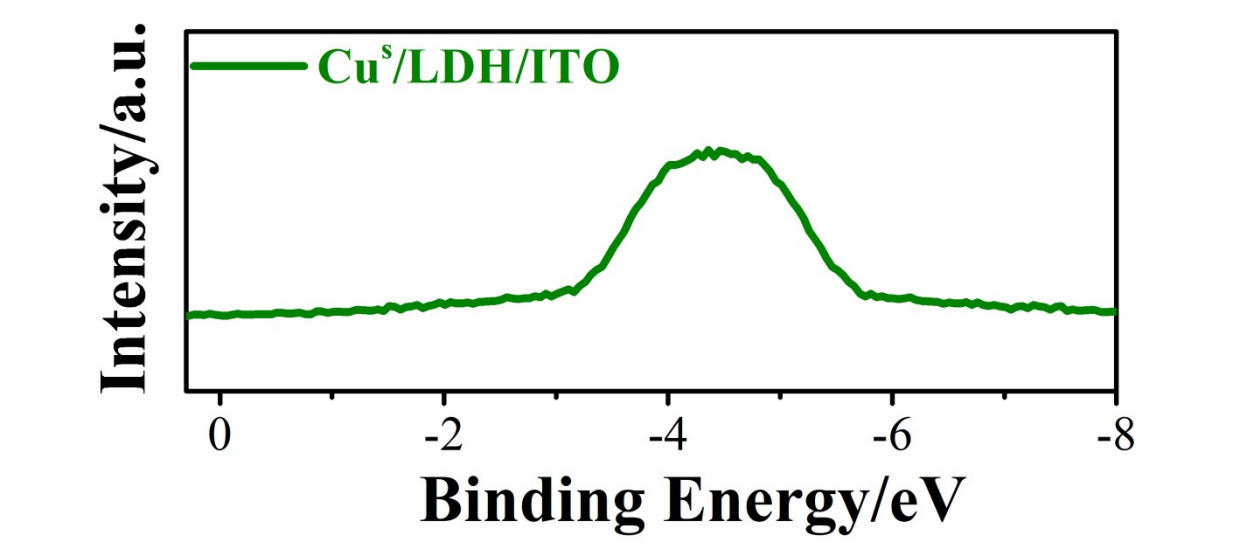

Fig. S20 Ultraviolet photoelectron spectroscopy (UPS) valence-band spectra of Cu^s/LDH/ITO.

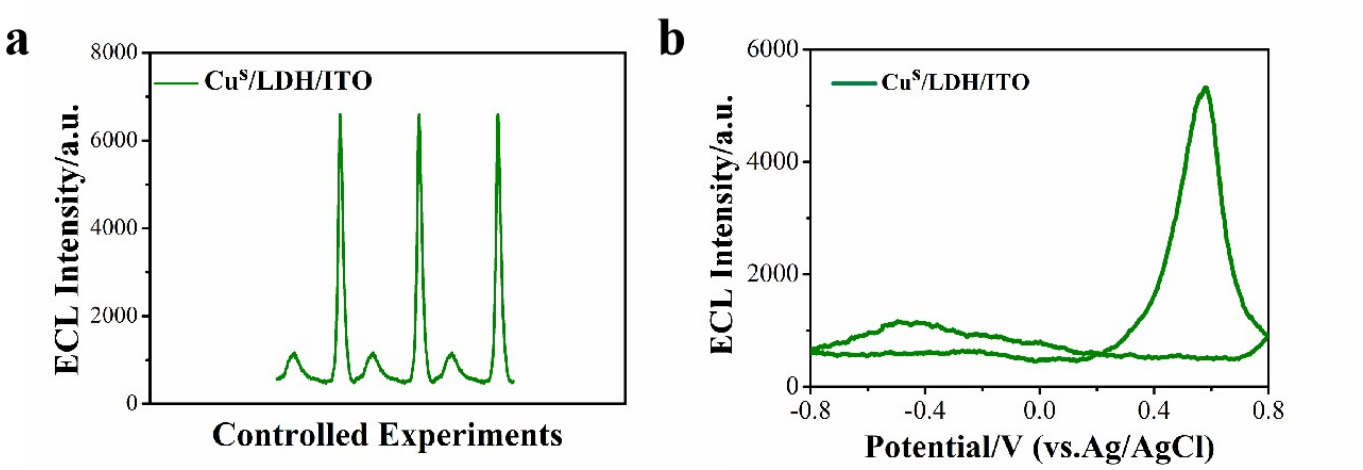

Fig. S21 (a) I_{ECL}-intensities and (b) I_{ECL}-potential curves for Cu^s/LDH/ITO sample.

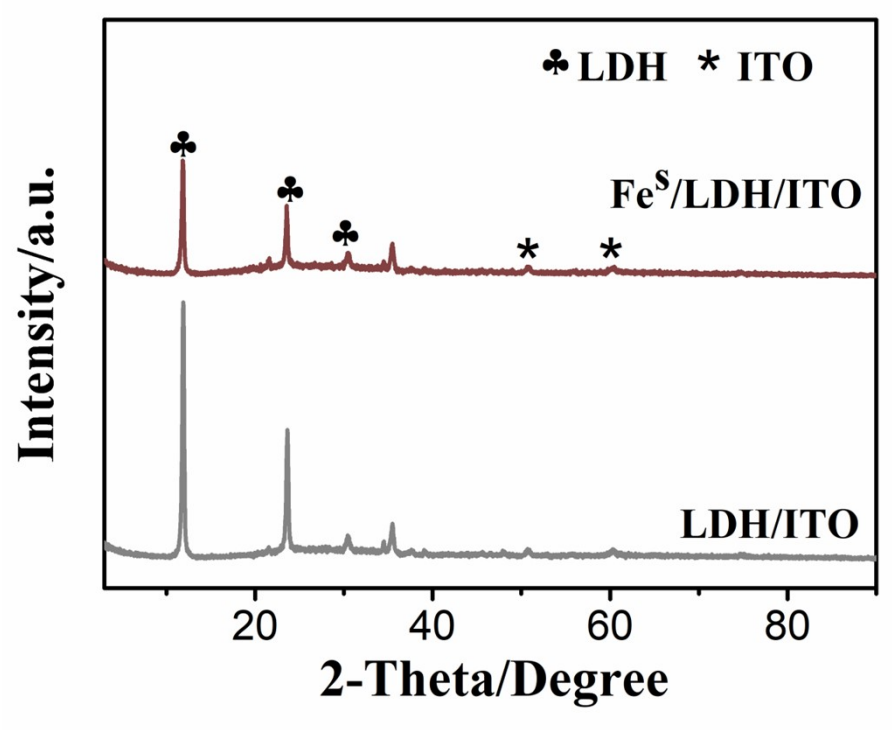

Fig. S22 XRD patterns of Fe^{s}/LDH/ITO and LDH/ITO samples (absence of Fe nanoparticles at 45°).

.

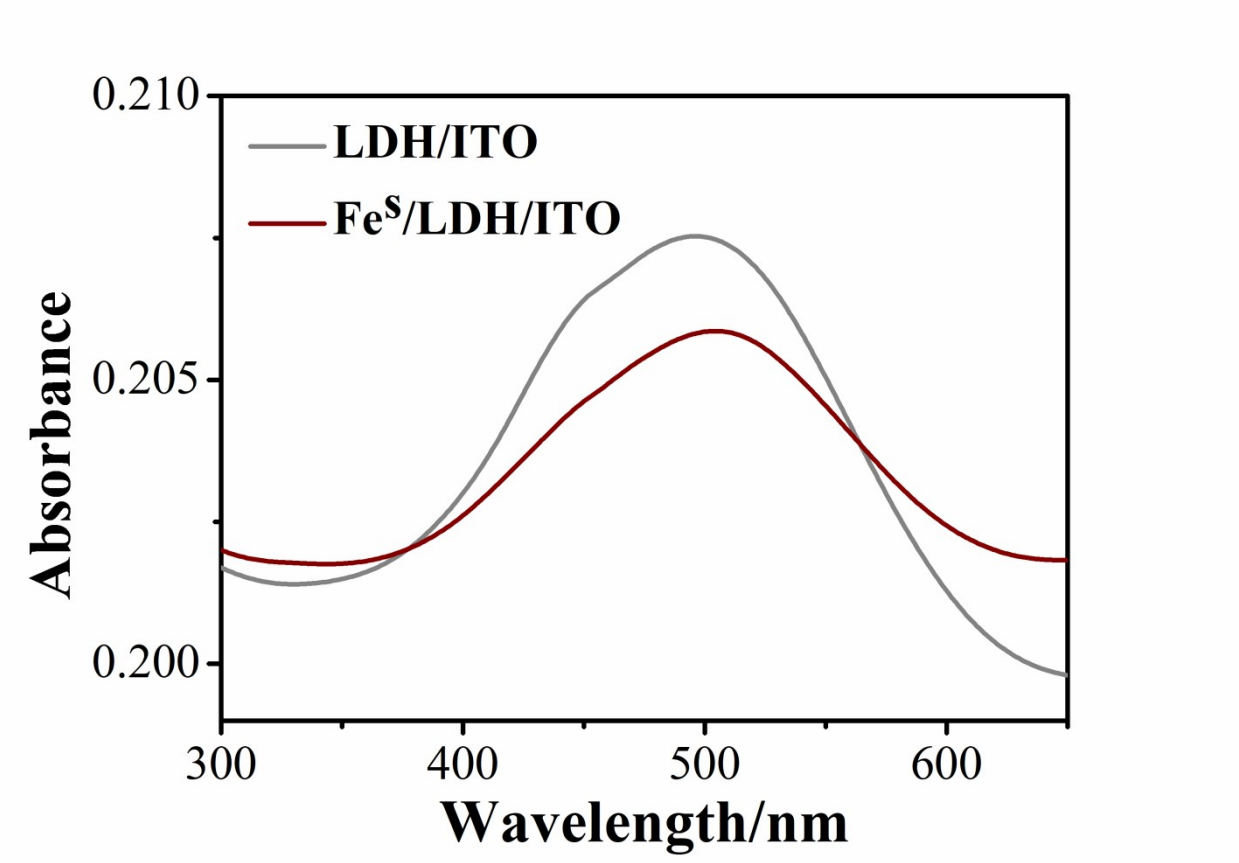

Fig. S23 UV-vis absorption spectra of Fe^{s}/LDH/ITO and LDH/ITO samples (absence of Fe nanoparticles at 400 nm).

.

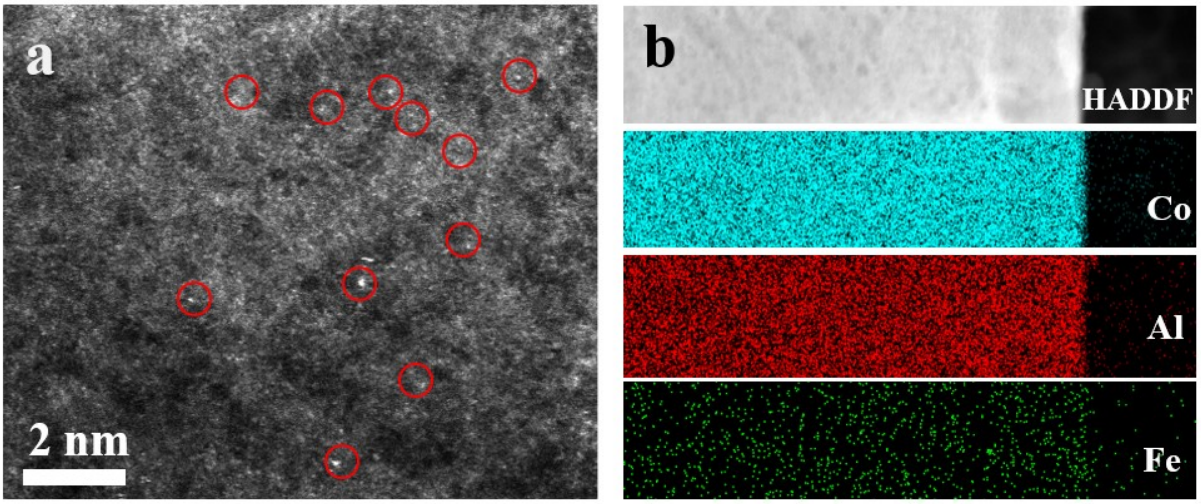

Fig. S24 (A) HAADF-STEM image and (B) STEM-EDS mapping images of Co, Al, and Fe for Fe^{s}/LDH/ITO.

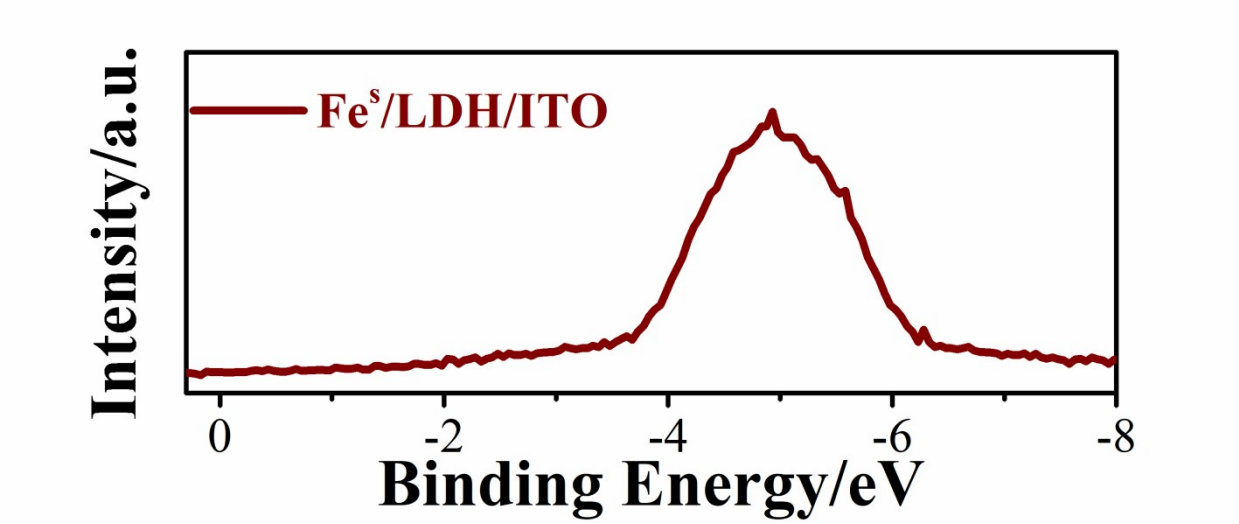

Fig. S25 UPS valence-band spectra of Fe^s/LDH/ITO.

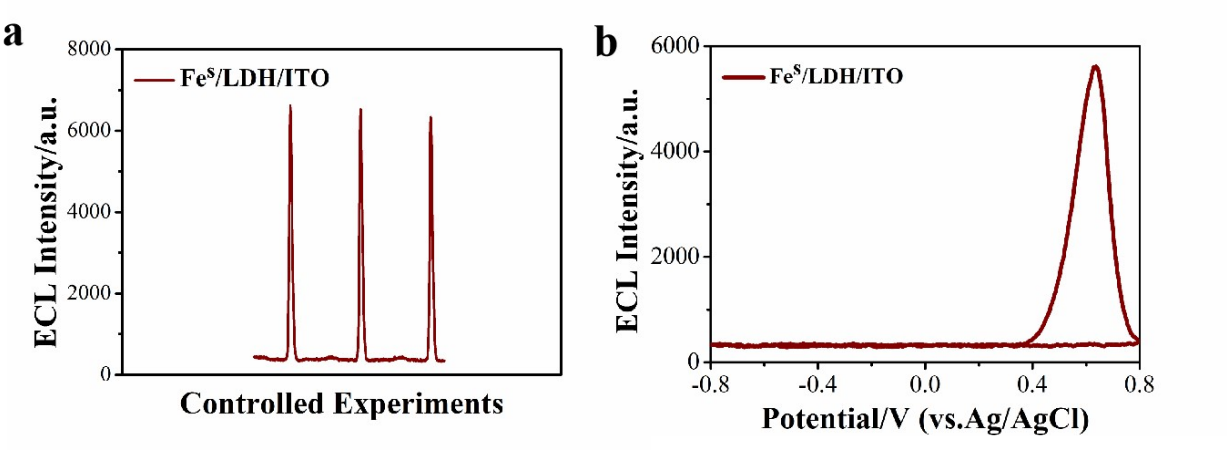

Fig. S26 (a) I_{ECL}-intensities and (b) I_{ECL}-potential curves for Fe^s/LDH/ITO sample.

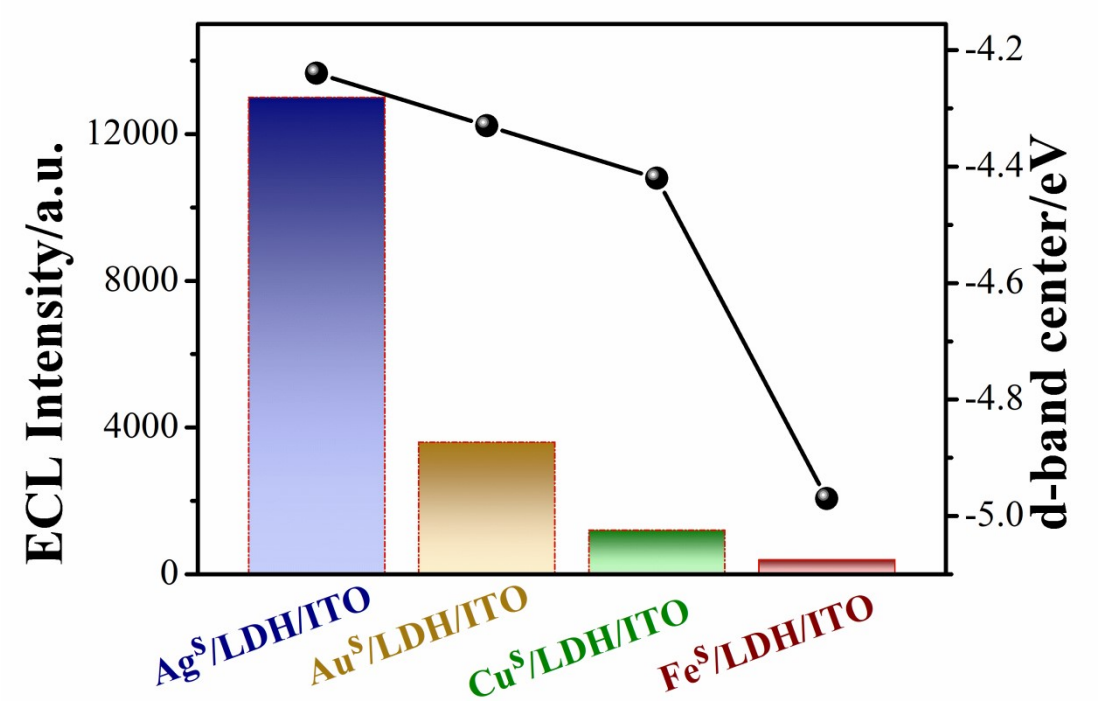

Fig. S27 Correlation between the d-band centers and ECL intensities of Ag^s/LDH/ITO, Au^s/LDH/ITO, Cu^s/LDH/ITO and Fe^s/LDH/ITO electrodes (ECL measurements were performed 0.01 mmol/L luminol, PBS, pH = 7.5).

The reaction of cathodic luminol ECL:

$O_2 \rightarrow$ ROSs

$LH_2 \rightarrow L^{\bullet-}$ (Dianion)

$L^{\bullet-}$ + ROSs $\rightarrow AP_2^{-*}$ (3-aminophthalate) $\rightarrow AP_2^{-} + h\nu$

The reaction of anodic luminol ECL:

$LH_2 + 2OH^- - 2e^- \rightarrow L^{\bullet-}$ (Dianion) + H_2O

$L^{\bullet-} + O_2^{\bullet-} \rightarrow LO_2^{2-}$ (5-amino phthalic acid) $\rightarrow AP_2^{-*}$(3-aminophthalate) + N_2

$AP_2^{-*} \rightarrow AP_2^{-} + h\nu$

Scheme S1. ECL mechanism of luminol catalyzed by the single-atom catalysts.

Table S1 Peak positions and Co^{3+}/Co^{2+} ratios of Co 2p in XPS spectra for LDH/ITO, Ag^{np}/LDH/ITO, Au^{np}/LDH/ITO, Ag^{s}/LDH/ITO and Au^{s}/LDH/ITO.

	Valence state	**Peak position (eV)**	**Relative contents (%)**	**Co^{3+}/Co^{2+} (%)**
LDH/ITO	Co^{3+}	783.7/798.8	23.3	71.9
	Co^{2+}	781.3/797.2	32.4	
Ag^{np}/LDH/ITO	Co^{3+}	783.6/798.4	36.3	70.3
	Co^{2+}	780.4/796.5	51.6	
Ag^{s}/LDH/ITO	Co^{3+}	783.2/798.1	17.6	40.6
	Co^{2+}	780.3/796.4	43.3	
Au^{np}/LDH/ITO	Co^{3+}	783.6/798.7	26.4	68.4
	Co^{2+}	780.9/797.0	38.6	
Au^{s}/LDH/ITO	Co^{3+}	783.5/798.2	26.3	65.4
	Co^{2+}	780.6/796.5	40.2	

Table S2 Information and calculation of the average oxidation states for Ag^s/LDH/ITO and Au^s/LDH/ITO.

Samples	Valence states	Integrated area	*C*%
Ag^s/LDH/ITO	Ag (0)	421.643	10%
	Ag (I)	3794.758	90%
Au^s/LDH/ITO	Au (0)	963.834	27%
	Au (I)	2605.922	73%

The calculations of the average oxidation states for single atomic Ag and Au were carried out according to the following equations:[3]

$Au_{oxidation\ state} = C\%Au(I) \times 1 + C\%Au(0) \times 0,$

$Ag_{oxidation\ state} = C\%Ag(I) \times 1 + C\%Ag(0) \times 0,$

where *C*% stood for the proportion of the integrated area for the different valence states to the total area calculated from the quantitative peak deconvolution.

Table S3 Peak positions and relative contents of O 1s in XPS spectra for LDH/ITO, Ag^s/LDH/ITO and Au^s/LDH/ITO.

	Oxygen species	**Peak position (eV)**	**Relative contents (%)**
LDH/ITO	O_H	533.8	20.1
	O_O	531.8	68.5
	O_{lat}	530.6	11.4
Au^s/LDH/ITO	O_H	532.9	10.7
	O_O	531.4	70.3
	O_{lat}	530.5	13.0
	Au–O	532.0	6.0
Ag^s/LDH/ITO	O_H	532.6	7.3
	O_O	531.3	71.2
	O_{lat}	530.4	14.0
	Ag–O	529.5	7.5

Table S4 ECL intensity variations of Au^s/LDH/ITO and Ag^s/LDH/ITO electrodes in the presence of different scavengers.

Samples	Radical scavengers	Target radicals	ECL intensity before addition	ECL intensity after addition	Quenching rates
Au^s/LDH/ITO	BQ	$O_2^{\bullet-}$	2.0×10^3	0.07×10^3	97%
	IPA	•OH	1.9×10^3	0.5×10^3	74%
	NaN_3	$^1O_2$	1.8×10^3	0.6×10^3	67%
Ag^s/LDH/ITO	BQ	$O_2^{\bullet-}$	2.6×10^4	0.2×10^3	99%
	IPA	•OH	2.3×10^4	2.6×10^3	89%
	NaN_3	$^1O_2$	2.4×10^4	3.0×10^3	87%

References

1 W. Shi, L. Bai, J. Guo and Y. Zhao, *RSC Adv.*, 2015, **5**, 89056-89061.

2 Z. Zhang, C. Feng, C. Liu, M. Zuo, L. Qin, X. Yan, Y. Xing, H. Li, R. Si, S. Zhou and J. Zeng, *Nat. Commun.*, 2020, **11**, 1215.

3 T. Kashyap, S. Biswasi, A. R. Pal and B. Choudhury, *ACS Sustain. Chem. Eng.*, 2019, **7**, 19295–19302.